energies

MDPI

Article

A Comparative Techno-Economic Analysis of Different Desalination Technologies in Off-Grid Islands †

Michael Castro, Myron Alcanzare, Eugene Esparcia, Jr. * and Joey Ocon *

Laboratory of Electrochemical Engineering (LEE), Department of Chemical Engineering, University of the Philippines Diliman, Diliman 1101, Philippines; mtcastro1@up.edu.ph (M.C.); mtalcanzare1@up.edu.ph (M.A.)

* Correspondence: eaesparcia@upd.edu.ph (E.E.J.); jdocon@up.edu.ph (J.O.)

† This paper is an extended version of our paper published in: Castro, M.T.; Esparcia, E.A.; Odulio, C.M.F.; Ocon, J.D. Technoeconomics of reverse osmosis as demand-side management for Philippine off-grid islands. *Chem. Eng. Trans.* **2019**, *76*, 1129–1134., also presented at 22nd Conference on Process Integration for Energy Saving and Pollution Reduction (PRES 19), Crete, Greece, 20–23 October 2019.

Received: 15 January 2020; Accepted: 23 April 2020; Published: 4 May 2020

Abstract: Freshwater in off-grid islands is sourced from rain, groundwater, or mainland imports, which are unreliable, limited, and expensive, respectively. Sustainable freshwater generation from desalination of abundant seawater is another alternative worth exploring. Model-based techno-economic simulations have focused on reverse osmosis desalination due to its low energy consumption and decreasing costs. However, reverse osmosis requires frequent and costly membrane replacement. Other desalination technologies have advantages such as less stringent feedwater requirements, but detailed studies are yet to be done. In this work, a techno-economic comparison of multi-effect distillation, multi-stage flash, mechanical vapor compression, and reverse osmosis coupled with solar photovoltaic-lithium ion-diesel hybrid system was performed by comparing power flows to study the interaction between energy and desalination components. Optimization with projected costs were then performed to investigate future trends. Lastly, we used stochastic generation and demand profiles to infer uncertainties in energy and desalination unit sizing. Reverse osmosis is favorable due to low energy and water costs, as well as possible compatibility with renewable energy systems. Multi-effect distillation and multi-stage flash may also be advantageous for low-risk applications due to system robustness.

Keywords: desalination; multi-effect distillation; multi-stage flash; mechanical vapor compression; reverse osmosis; renewable energy

1. Introduction

Small off-grid islands have costly, limited, and intermittent supply of electricity and water due to dependence on importation. In the case of the Philippines, they are often electrified by diesel generators that are supplied with diesel imported from the mainland, resulting in high electricity prices (i.e., six times that of the mainland) because of high transportation costs [1]. In addition, freshwater for general purposes on these islands is sourced from an unreliable rainwater supply or a limited and vulnerable groundwater source [2]. Drinking water may be imported from the mainland at a cost of around 1 USD/L [3]. Economic activity on these islands are adversely affected as a result of the high costs of electricity and water. In particular, the International Labor Organization identified that freshwater scarcity hinders economic growth, as businesses would compete with residents for the resource [4]. The scarcity of clean freshwater can be solved through seawater desalination, but it is

energy intensive [5]. Putting additional conventional power generation capacity must be considered alongside desalination capacity, but this may be an unsustainable and more costly option [1]. In contrast, putting up renewable energy (RE) generation capacity to augment desalination may be more feasible because of the decreasing costs of solar photovoltaic (PV) [6] and battery energy storage systems (BESS) [7]. Hybrid energy systems consisting of solar PV, diesel generators, and energy storage were shown to reduce electricity costs in off-grid areas [8]. In the Philippines, Ocon and Bertheau estimated a 20% energy generation cost reduction for Philippine off-grid islands upon transition from a diesel-only system to a solar PV-based hybrid system [1], while Bertheau and Blechinger considered a 10-year load growth in their analysis and found the same trend [9]. Note that the works mentioned were focused on finding the lowest levelized cost of electricity only.

Table 1 summarizes the literatures that conducted feasibility studies for both energy and desalination systems. Some works have focus on the optimal combination of components. For example, Fernández-Gil and Petrakopoulou showed that implementing RE-desalination systems on Skyros Island, Greece yields freshwater at a cost of 2.75 USD/m^3, which is 52% lower than imported freshwater [10]. Tafech et al. show that reverse osmosis (RO) powered by a PV-wind system can yield freshwater at a cost of 1.87 USD/m^3 on King Island, Australia [11]. For comparison, the freshwater cost in those literatures reviewed are more expensive than that of mainland Philippine water cost which amounts to 0.70 USD/m^3 [12]. Other works focused on dispatch algorithms. For instance, Gökçek simulated solar PV, wind, and diesel-based energy systems coupled with RO as an additional electrical load [13]. Corsini and Tortora demonstrated the load leveling capabilities of RO by absorbing excess RE generation in a PV-diesel hybrid system [14]. Lastly, Bognar et al. compared different RO dispatch strategies which shows both energy and water generation costs may be minimized by treating RO as a deferrable load [15]. Note that excessive desalination turndown could arise, which will damage the desalination plant [16].

Table 1. Summary of energy-desalination feasibility studies. RO: reverse osmosis; PV: photovoltaic.

Ref.	Energy				Desalination		Remarks
	PV	Wind	Diesel	Batt	RO	Other	
[17]	✓	✓	✓		✓		• Case study in off-grid areas in Iraq • Solar-wind-diesel-RO system has lowest water generation costs
[11]	✓	✓	✓	✓	✓		• Case study based on King Island, Australia • Solar PV-RO has the lowest water generation cost • Water storage important for dealing with uncertainties
[18]	✓	✓			✓		• Case study in Algarve, Portugal • Decentralized system yields lowest generation cost
[19]					✓	✓	• Economic feasibility of supplying water demand of US coastline via RO • US electricity consumption will increase by only 0.5%
[10]					✓	✓	• Case study in Skyros, Greece • Freshwater generated from desalination is cheaper than imported freshwater
[20]					✓		• Compared different brackish water RO methods • Batch and closed-circuit desalination designs are energy efficient
[21]		✓			✓		• Analyzed the use of desalinated water for agriculture • Case study in Canary Islands, Spain

Table 2 compares different desalination technologies from different works in the literature, which generally shows insufficient technical detail. In contrast, research listed in Table 1 involve rigorous

model-based simulations, but are mostly limited to RO. This is not surprising considering that the technology has a low energy consumption [19] and decreasing investment costs [22], making it practical for installation. The technology constitutes the largest share of installed global desalination capacity with 69% of the global desalinated water production [23].

Table 2. Review of comparative desalination studies. MED: multi-effect distillation; MSF: multi-stage flash; MVC: mechanical vapor compression.

Ref.	Desalination				Remarks
	MED	MSF	MVC	RO	
[24]	✓	✓	✓	✓	• Discusses merits of other technologies • MED needs less pretreatment than RO • MVC has more compact installations
[25]	✓	✓	✓	✓	• Review of costing methodologies • Correlate desalination cost with installed capacity or growth rate
[26]	✓	✓		✓	• Parameters for logistic growth curves of cumulative installed capacity
[27]					• Estimated 29% learning rate [1] between desalination cost and cumulative installed capacity • Not specific to any desalination method
[22]				✓	• Estimated 15% learning rate [1] for RO
[28]	✓			✓	• Compared MED, RO, and novel capillary-driven desalination (CDD) • CDD has good balance between energy consumption and water production

[1] Learning rate in these studies refers to the percentage by which the cost of desalination decreases when the cumulative installed capacity doubles. Other definitions, such as those based on the doubling of cumulative generation, also exist [29].

RO is a membrane-based desalination technology in which saltwater passes through a semipermeable membrane that blocks ions and other contaminants. Freshwater is collected at the other end of the membrane [5]. In a continuous process, the feedwater channel, membrane, and freshwater permeate collectors are pressed and wound in a cylindrical package (Figure 1). At the center of the cylinder is the permeate tube with freshwater [30]. Despite its advantages, the technology is still hindered by frequent membrane degradation [31]. Many works have tackled the technical issue by using different membrane types [32] and managing membrane fouling [33]. This has led some studies to consider other desalination methods. Other membrane-based technologies include electrodialysis (ED), wherein saltwater is passed between alternating layers of anodic and cathodic exchange membranes. These membranes allow only anions and cations to pass, respectively. Ions are separated and trapped between every other layer when an electric field is applied, forming alternating layers of freshwater and brine [34].

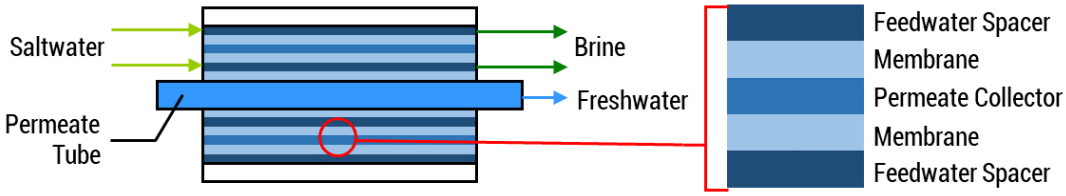

Figure 1. Reverse Osmosis (RO).

Thermal desalination systems generally produce freshwater from the vapors of heated saltwater [24]. An example is multi-effect distillation (MED, Figure 2). Saltwater is placed in a series of heat exchange vessels. The first stage receives external heating and some steam is produced. This steam serves as the heat source of the next stage and is collected as freshwater upon condensing. This is repeated across several stages. At the final stage, the steam preheats the feed saltwater before condensing [35]. Another thermal desalination system is multi-stage flash (MSF, Figure 3) [36]. The saltwater is heated using recovered heat and external heating sources. It is then flashed at the first stage to produce steam and concentrated saltwater. The steam condenses after heating the feed saltwater. The condensate is collected as freshwater. The concentrated saltwater is flashed at a lower pressure in the next stage. In mechanical vapor compression (MVC, Figure 4) [37], saltwater partially vaporizes in a closed vessel. The vapors are passed into a compressor, which raises the temperature of the vapor stream. Heat is then exchanged with the saltwater in the feed and the vessel to produce more vapor. Although this technology is classified as a thermal process, it does not use external heating sources [38]. MSF and MED constitute 18% and 7% of the global desalinated water generation, respectively [23].

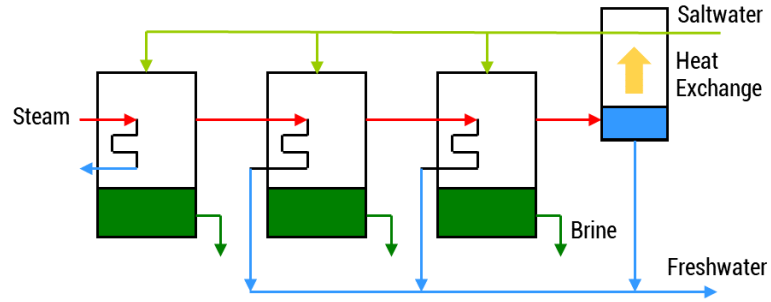

Figure 2. Multi-effect distillation (MED).

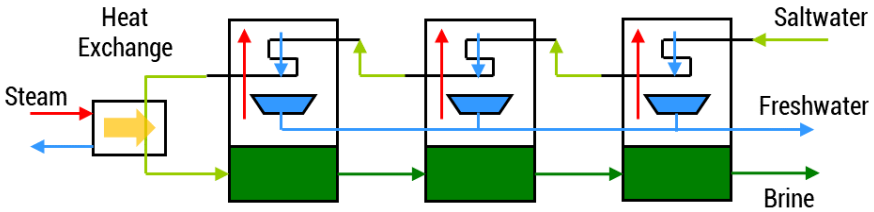

Figure 3. Multi-stage flash (MSF).

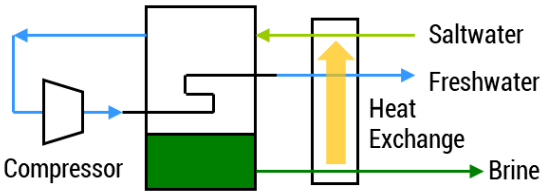

Figure 4. Mechanical vapor compression (MVC).

Performing techno-economic studies to integrate water desalination to the off-grid energy systems requires accurate models [39], while different economic dispatch algorithms must be tested as they generate varying results. In addition, results that use deterministic generation and demand profiles such as the literatures reviewed may not be accurate due to uncertainties in demand and/or RE generation [40]. Lastly, results that use constant cost over time may also not be accurate as it is expected that desalination costs will decrease as the technology matures [26]. For the Philippine context, Castro et al. have reviewed different RO dispatch algorithms. The results suggest that treating RO as a sink while demanding additional generation when water storage is low can minimize water generation costs [41]. However, testing the techno-economic feasibility of different desalination technologies under different economic dispatch algorithms while accounting stochastic behavior of generation and demand profiles and projected decreasing technology has not been done yet.

In this work, a techno-economic comparison of MED, MSF, MVC, and RO desalination coupled to a solar PV-diesel hybrid system with lithium ion (Li-ion) BESS is performed. The desalination technologies were selected based on their commercial maturity. The analysis of the desalination technologies was divided into four parts. First, the optimum sizes of energy and desalination components and their uncertainties were determined using stochastic generation and demand profiles. Second, power flows were generated to investigate the interaction between energy and desalination components. Third, energy and water generation costs were calculated at different starting periods to analyze the risks and tradeoffs of delaying plant construction. Lastly, a sensitivity analysis of optimum sizes to the overnight diesel and coal cost was conducted to account for uncertainties in diesel prices.

2. Materials and Methods

2.1. System Architecture

The coupling of the energy and water system is shown in Figure 5. The energy system supplies both the electrical demand of the island and the desalination unit. The electrical demand of the desalination system depends on the water storage level and is discussed further in Section 2.3. If excess RE generation is present, it is dispatched to the desalination system to generate more water. The generated water is sent to the water storage, from where the water demand is drawn. Details on the operation of the energy system is shown in Appendix A.

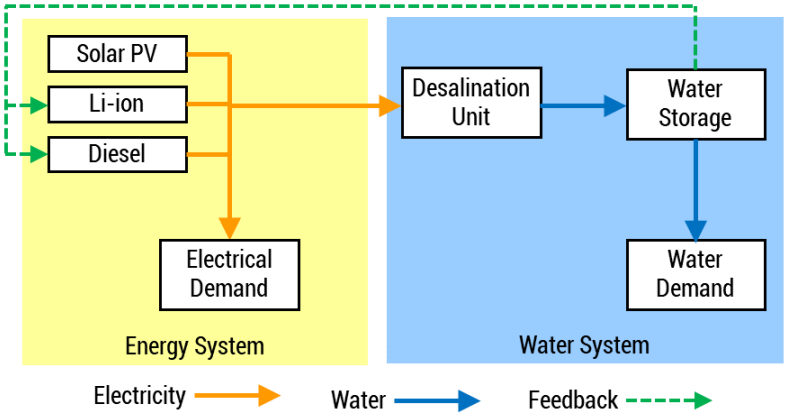

Figure 5. Architecture of the coupled energy and water system.

2.2. Modelling Approach

The calculations were performed using Island System $LCOE_{min}$ Algorithm (ISLA), an in-house microgrid optimization software written in Python 3. The solar PV, diesel, Li-ion BESS, and desalination modules in ISLA were used. Microgrid energy system optimizations were validated with HOMER Pro® (HOMER Energy LLC: Golden, CO, USA). The software simulates the interaction of energy

and water components for one representative year in hourly resolution and calculates the levelized cost of electricity (LCOE), levelized cost of water (LCOW), and net present costs (NPC) as shown in Equations (1)–(3), respectively [42]:

$$\text{LCOE} = \frac{\text{CRF} \cdot \sum_{\text{el}} C_i}{\sum_{t=0}^{8759} P_{ld}(t)\Delta t}, \tag{1}$$

$$\text{LCOW} = \frac{\text{CRF} \cdot \sum_{\text{wt}} C_i + \text{LCOE} \cdot \sum_{t=0}^{8759} P_{de}(t)\Delta t}{\sum_{t=0}^{8759} \dot{V}_{ld}(t)\Delta t}, \tag{2}$$

$$\text{NPC} = \sum C_i, \tag{3}$$

In the equations above, $P_{ld}(t)$ is the electrical load, $\dot{V}_{ld}(t)$ is the water demand, $P_{de}(t)$ is the power entering the desalination unit, $\sum_{\text{el}} C_i$ is the total annualized cost of electrical components, $\sum_{\text{wt}} C_i$ is the total annualized cost of water components, and $\sum C_i$ is the total annualized cost of all components. The capital recovery factor (CRF) is defined in Equation (4), wherein i is the discount rate and t_s is the project lifetime [y] [42]:

$$\text{CRF} = \frac{i(1+i)^{t_s}}{(1+i)^{t_s} - 1}, \tag{4}$$

ISLA finds the component sizes S_i that minimize the NPC as shown in Equation (5). The optimization is constrained such that both electricity and water demand are always satisfied during the representative year. These are formalized in Equations (6) and (7). In these equations, $P_{PV}(t)$, $P_{Li}(t)$, and $P_{ds}(t)$ are the power outputs of solar PV, Li-ion BESS, and diesel genset, respectively. $V_{tank}(t)$ is the volume of water in storage. These variables are subject to additional constraints based on the component models and sizes S_i. The models for energy and water components are discussed in Appendix A and Section 2.3, respectively.

$$\text{minNPC}(S_i), \tag{5}$$

$$P_{PV}(t) + P_{Li}(t) + P_{ds}(t) \geq P_{ld}(t) + P_{de}(t) \quad \forall t \in [0,\ 8759],\ t \in \mathbb{N}\ , \tag{6}$$

$$V_{tank}(t) \geq \dot{V}_{ld}(t)\Delta t \quad \forall t \in [0,\ 8759],\ t \in \mathbb{N}\ , \tag{7}$$

The optimization process is performed using an iterative search space algorithm as demonstrated in Figure 6. Sets of component sizes are generated, and the NPC of each combination is calculated. The combination with the lowest NPC is selected, and a finer search space is generated from this combination. The generation of the initial search space is crucial to obtain a proper optimum value, which is discussed further in Appendix B.

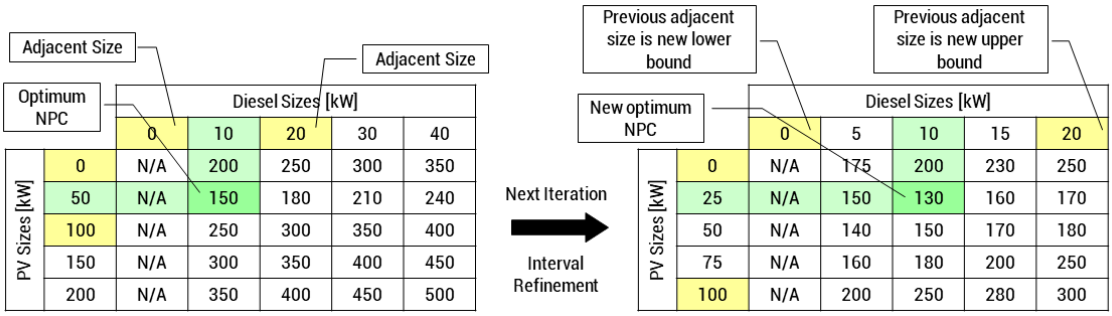

Figure 6. Iterative search space algorithm used by Island System LCOE_{min} Algorithm (ISLA) on a hypothetical PV-Diesel system. N/A values in the figure indicate a technically infeasible system and are ignored. LCOE: levelized cost of electricity.

2.3. Desalination Model

The energy required for a desalination plant to generate one volumetric unit of freshwater is defined as the energy intensity (EI). It is divided into electrical energy intensity (EI_{el}) for mechanical processes and a thermal energy intensity (EI_{th}) for heating processes [19]. MVC and RO, which do not have external heating, have zero EI_{th} [19]. Equation (8) relates the EI_{el} to the water generated $\dot{V}_{de}(t)$ and the electrical power entering the desalination plant $P_{de}(t)$ at time t. For desalination technologies that require external heating, the mass of coal used $\dot{m}_{cl}(t)$ [kg/h] is given by Equation (9), wherein ΔH is the lower heating value of coal (17.89 MJ/kg) [43]:

$$\dot{V}_{de}(t) = \frac{P_{de}(t)}{EI_{el}}, \tag{8}$$

$$\dot{m}_{cl}(t) = \frac{P_{de}(t)}{\Delta H} \times \frac{EI_{th}}{EI_{el}}, \tag{9}$$

The generated water is then sent to a storage tank, where the water demanded is simultaneously drawn. This is summarized by Equation (10), wherein $V(t)$ is the volume of water in the tank, $\dot{V}_{ld}(t)$ is the water demand, and Δt is the simulation time step (1 h):

$$V(t + \Delta t) = V(t) + \left[\dot{V}_{de}(t) - \dot{V}_{ld}(t)\right]\Delta t, \tag{10}$$

The power that enters the desalination plant depends on the water level. If the water level is above 20%, then the minimum power requirement $P_{de}^{min}(t)$ depends on the turndown ratio (TDR). The TDR is the ratio between minimum and rated production, and operation below this point will damage the desalination plant. If the water level is below 20%, the minimum power requirement will be set to restore the water level to at least 20%. This is summarized by Equation (11), wherein V_{tank} is the volume of the storage tank:

$$P_{de}^{min}(t) = \begin{cases} \text{TDR} \cdot S_{de} & V(t) \geq 0.2V_{tank} \\ \frac{EI_{el}}{\Delta t}\left(0.2 - \frac{V(t)}{V_{tank}}\right) & V(t) < 0.2V_{tank} \end{cases}, \tag{11}$$

The EI and TDR of the considered desalination technologies are shown in Table 3.

Table 3. Energy intensity (EI) and turndown ratio (TDR) of desalination technologies.

Desalination	EI_{el} [kWh/m^3]	Ref.	EI_{th} [kWh/m^3]	Ref.	TDR	Ref.
MED	2.50	[44–46]	53.20	[44,45]	0.50	[47]
MSF	4.17	[44–46]	64.79	[44,45]	0.70	[48]
MVC	12.41	[19,45]	-	[19,44]	0.50	[49]
RO	4.35	[19,44,45]	-	[19,44]	0.33	[50]

2.4. Techno-Economic Assumptions

The techno-economic parameters as of 2015 of each desalination technology are shown in Table 4. The operating costs were adjusted so that electrical and thermal requirements were excluded, as these were modeled explicitly. The techno-economic parameters of the energy components are shown in Appendix C.

Table 4. Techno-economic parameters of desalination technologies.

Component	Parameter	Unit	Value	Ref.
MED	CapEx	USD/(m^3/d)	1150	[25,46]
	OpEx	USD/m^3	0.232	[25]
	Lifetime	y	6	[31]
MSF	CapEx	USD/(m^3/d)	1425	[25,46]
	OpEx	USD/m^3	0.232	[25]
	Lifetime	y	10	[51]
MVC	CapEx	USD/(m^3/d)	1000	[52]
	OpEx	USD/m^3	0.232	[25]
	Lifetime	y	10	[51]
RO	CapEx	USD/(m^3/d)	1250	[25,46]
	OpEx	USD/m^3	0.232	[25]
	Lifetime	y	10	[51]
Water Storage	CapEx	USD/m^3	1000	[13]
	OpEx	USD/m^3/y	10	
	Lifetime	y	20	
Coal	Unit Cost	USD/kg	0.09	[53,54]
	Inflation Rate	%	3	

2.5. Future Costs

The capital cost of a desalination technology $C_{cap}(t)$ at year t is given by Equation (12). The capital cost decreases with the cumulative installed capacity $X(t)$ given by Equation (13). In these equations, a is a normalization constant, b is an empirical parameter based on learning rates, K is the saturation capacity, r is the growth rate, and t_m is the year when half of the saturation capacity is installed [26]. The parameter values for each desalination technology are given in Table 5, while the future cost parameters for energy components are shown in Appendix D.

$$\frac{C_{cap}(t)}{C_{cap}(2015)} = a[X(t)]^{-b}, \tag{12}$$

$$X(t) = \frac{K}{1 + exp[-r(t - t_m)]}, \tag{13}$$

Table 5. Future cost parameters of desalination technologies.

Component	K [GW(h)]	r [y^{-1}]	t_m [y]	Ref.	b	Ref.
MED	10.30	0.1126	2011	[26]	0.3771	[55]
MSF	21.10	0.0935	1999	[26]	0.5146	[55]
MVC	0.24	0.1888	1966	[56]	0.4941	[27]
RO	147.20	0.1256	2019	[22]	0.2345	[22]

2.6. Case Study

In this work, Camasusu Island, Masbate (12.2 °N; 123.2 °E) and Lubang Island, Occidental Mindoro (13.8 °N; 120.1 °E) in the Philippines are selected as case studies to represent small and big islands, respectively. The daily water demand profiles were estimated from the work of the California Public Utilities Commission [57], with monthly variations based on Griffin and Chang [58]. The resulting water demand profiles were scaled to meet the 20-L water requirement per day per capita estimate by the World Health Organization [56]. Camasusu and Lubang Island have a population of 532 and 18,556, respectively, which yields an annual water demand of 3.88×10^3 m^3/y and 1.35×10^5 m^3/y. This

estimate includes water for drinking and activities such as bathing and laundry [56]. The normalized water demand profile is shown in Figure 7. The details regarding demand and generation profiles of the energy components are given in Appendix E.

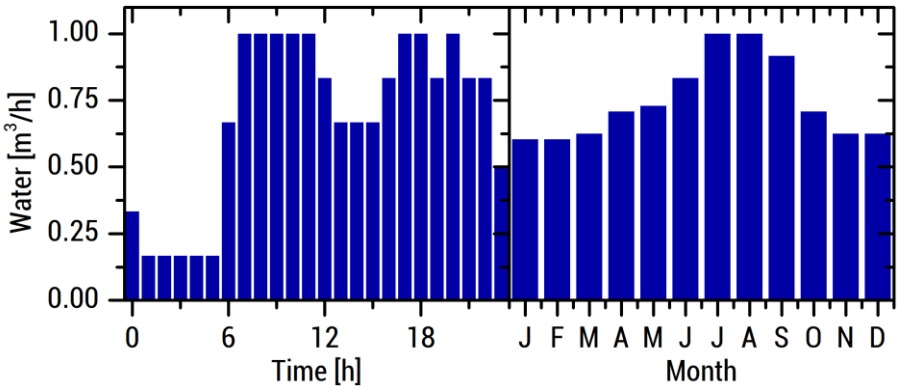

Figure 7. Normalized water demand profile. This is scaled up to match the annual demand. The left panel shows the daily average demand in hourly resolution, while the right panel shows the monthly variation over a year.

2.7. Stochastic Profile Generation

Stochastic energy and water demand profiles were generated using Equations (14) and (15). In these equations, $P_{ld}(t)$ and $\dot{V}_{ld}(t)$ are the deterministic energy and water profiles, $\delta_{hr}(t)$ is a random number that varies every hour, and $\delta_{dy}(t)$ varies every day. Both random numbers are drawn from a normal distribution centered at 0 with 5% variance. Generation of the stochastic hourly solar insolation profiles are discussed by Bendt et al. in [59] and Graham et al. in [60,61].

$$P_{ld}^{stoc}(t) = P_{ld}(t)\Big[1 + \delta_{hr}(t) + \delta_{dy}(t)\Big], \tag{14}$$

$$\dot{V}_{ld}^{stoc}(t) = \dot{V}_{ld}(t)\Big[1 + \delta_{hr}(t) + \delta_{dy}(t)\Big], \tag{15}$$

After each set of generation and demand profiles are formed, a Monte-Carlo approach calculated the corresponding optimum sizes and metrics 100 times to determine their distribution. The number of simulation points were chosen to balance computation time and accuracy.

3. Results

3.1. Optimum Sizes

Figures 8–10 present the results of the Monte-Carlo simulation. Figure 8 shows that diesel-favored systems need less energy storage capacity, while solar PV-favored systems will need larger Li-ion BESS capacities. For these hybrid systems, larger Li-ion BESS sizes indicate higher RE shares. Bimodal distributions indicate the possibility of either RE-favored generation or diesel-favored generation. Figure 8 also presents that low energy and water demand on an island such as in Camasusu would result in diesel-favored generation systems, as the installation costs for diesel-favored generations are lower than that of RE. At low energy demands, the large installation cost required makes RE less economical than diesel-generation. In contrast, larger islands with more energy and water demands such as in Lubang prefer RE-favored systems. On these islands, the large installation cost of RE is offset by the decreased fuel consumption.

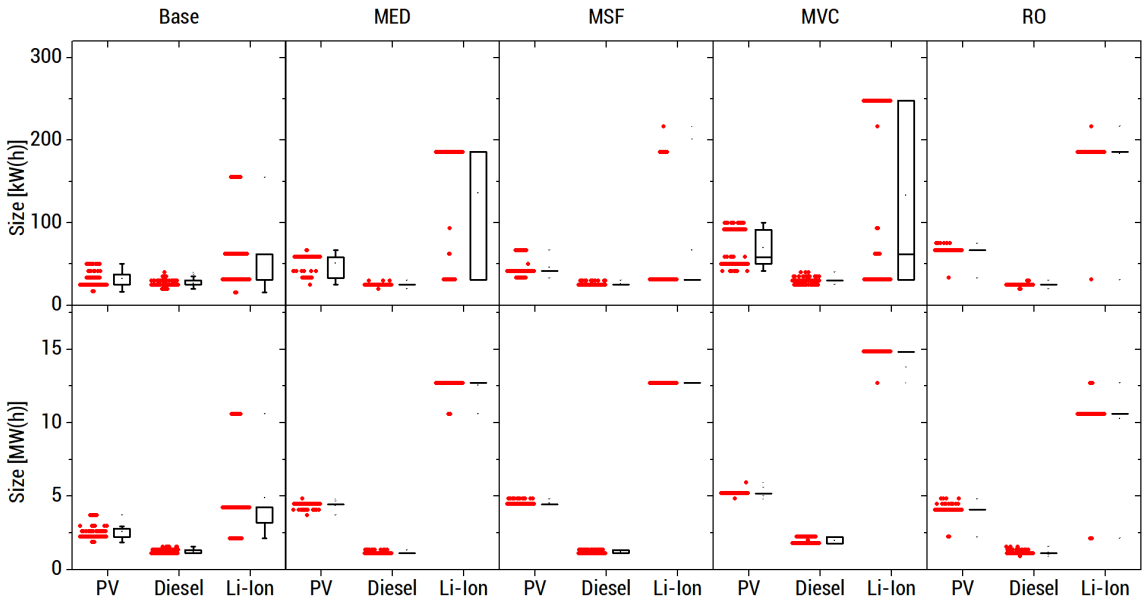

Figure 8. Distribution of optimum sizes of energy components on Camasusu Island (**top**) and Lubang Island (**bottom**). Systems in Camasusu have small Li-ion BESS installation sizes, except for RO, where the Li-ion BESS installation is large. Systems in Lubang have large Li-ion BESS installations.

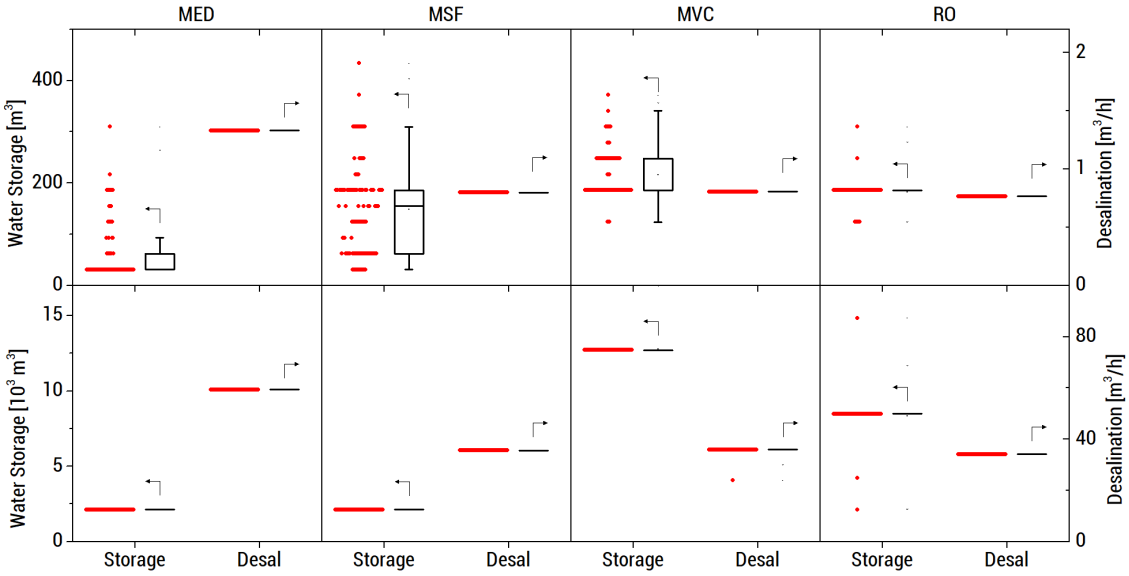

Figure 9. Distribution of optimum sizes of water storage (**left** axis) and desalination unit (**right** axis) on Camasusu Island (**top**) and Lubang Island (**bottom**). There is high uncertainty in the optimum water storage sizes in Camasusu, except for RO.

Figure 9 shows how diesel-dominated systems compensate for the lack of Li-ion BESS capacity. As these systems do not have energy storage, they use the desalination plant as an energy sink to produce and store water that will be utilized daily. The same figure presents that if the desalination plant is used as an energy sink, the resulting storage sizes for water have large uncertainty or spread. The RO system in Camasusu is an exception to the trends observed earlier. RO has a high turndown capability that allows RE intermittence as seen in the spread between solar PV and Li-ion BESS installation in Figure 8. In cases where RE is heavily preferred over diesel-generators, RO systems are suggested for small islands.

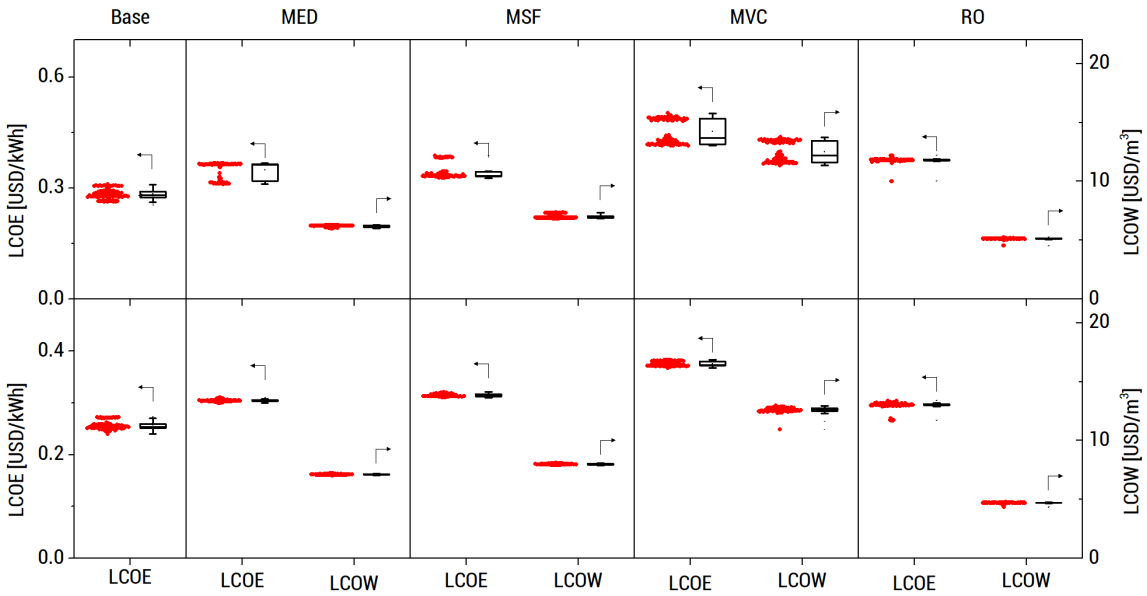

Figure 10. Distribution of optimum LCOE (**left** axis) and levelized cost of water (LCOW) (**right** axis) on Camasusu Island (**top**) and Lubang Island (**bottom**). The metrics of the MED and MVC systems in Camasusu exhibit a bimodal distribution.

As for the optimum metrics shown in Figure 10, RO desalination provides the lowest water generation costs from its low energy intensity and fuel independence. Electricity generation costs are comparable for MED, MSF, and RO because the corresponding desalination unit has low electricity consumption, although MED may achieve a lower cost. The larger Lubang Island has lower generation costs than Camasusu Island, further demonstrating the effectiveness of RE systems on larger islands. Figure 10 also reflects the importance of desalination turndown on the stability of generation costs. RO systems have a more distinct generation cost distribution because shortage in generation due to intermittencies is allowed by larger turndown; thus, additional generation capacity and the associated costs are unnecessary. In other systems, however, turndown is limited and therefore, intermittency is met with additional generation capacity. The amount of additional generation is unpredictable, and this reflects as uncertainties in generation costs.

3.2. *Hourly Power and Water Flows*

Figure 11 shows the power flows of a representative day associated with each desalination technology coupled with hybrid energy systems on both islands. The power flows confirm that systems on Camasusu Island are diesel-favored, while those on Lubang Island are RE-favored. An exception is the RO system on Camasusu Island, which uses an RE-favored system because of its high turndown capability. The diesel-favored systems have batteries that drain to 20% outside of sun-hours, which result in diesel generation to meet the baseload. In contrast, the RE-favored systems only utilize diesel generation during days with low solar irradiation.

Figure 12 compares the power consumed by the different desalination units and demonstrates how water is stored. In MED and MSF, water output is continuous because of the low turndown, increasing water level over time. In RO systems, however, water storage is drained until it reaches the minimum water level. After this, the RO plant will start producing water to meet the demand, explaining the uneven energy demand profile. Because of this, the RO system behaves as an additional load during the day. This is evidenced by the monthly average water level shown in Figure 13 wherein MED and MSF water storage tanks are full, while RO water storage is minimum.

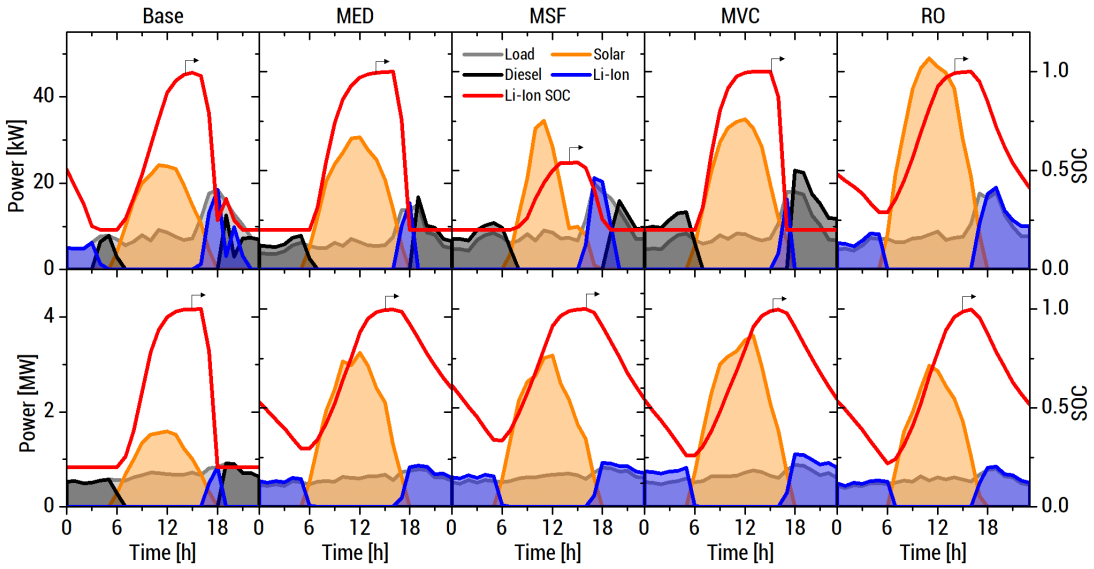

Figure 11. Hourly power output of electrical components and Li-ion BESS state of charge (SOC) on Camasusu Island (**top**) and Lubang Island (**bottom**). Li-ion BESS usage is high on Lubang Island.

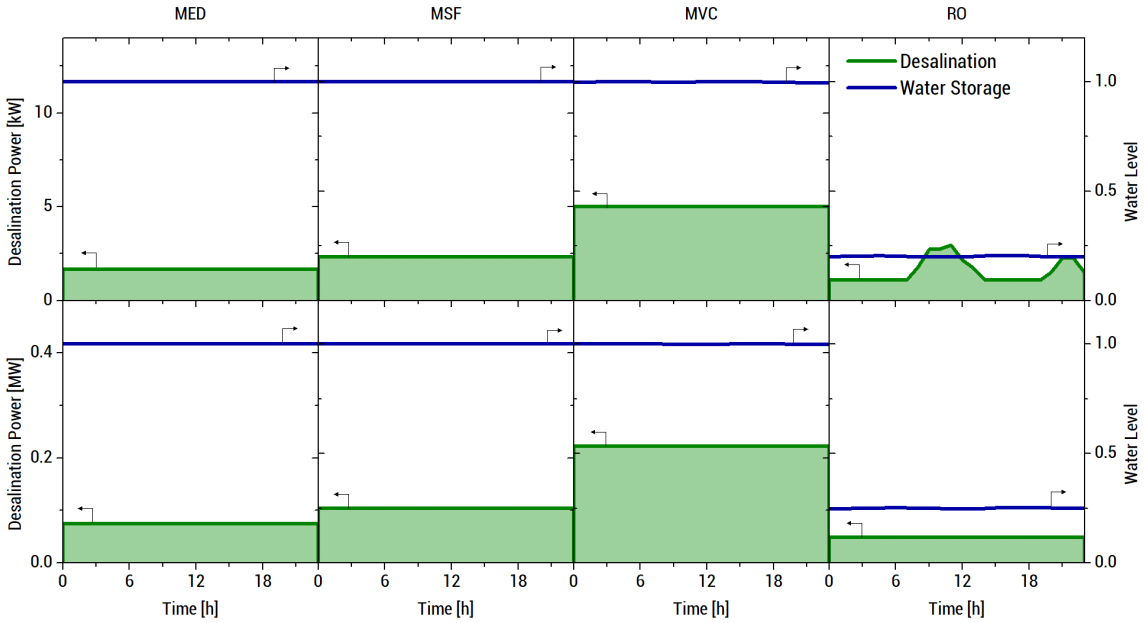

Figure 12. Hourly desalination energy consumption and water storage fraction on Camasusu Island (**top**) and Lubang Island (**bottom**). Power consumption is uneven in the RO system on Camasusu Island.

3.3. Future LCOE and LCOW

Figure 14 shows the projected LCOE and LCOW of one representative case for both islands from 2015 to 2050. Note that the LCOE and LCOW of a particular year does not account construction time. The results suggest that RO will provide the lowest water generation costs, followed by MED and MSF. MED, MSF, and RO have comparable electricity generation costs, which is also suggested by Figure 10. The systems in Camasusu and the MVC system in Lubang have a small price spike. This suggests a transition to RE-favored generation in the future.

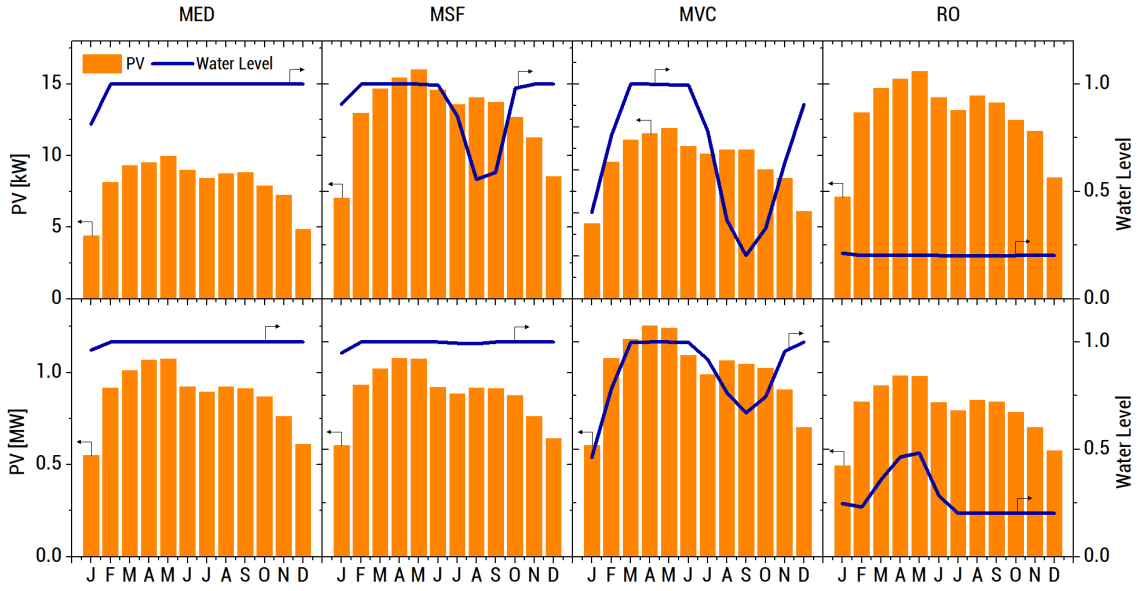

Figure 13. Monthly average PV power and water level on Camasusu Island (**top**) and Lubang Island (**bottom**). Note that stability of the system is ensured due to an imposed minimum water level of 20%.

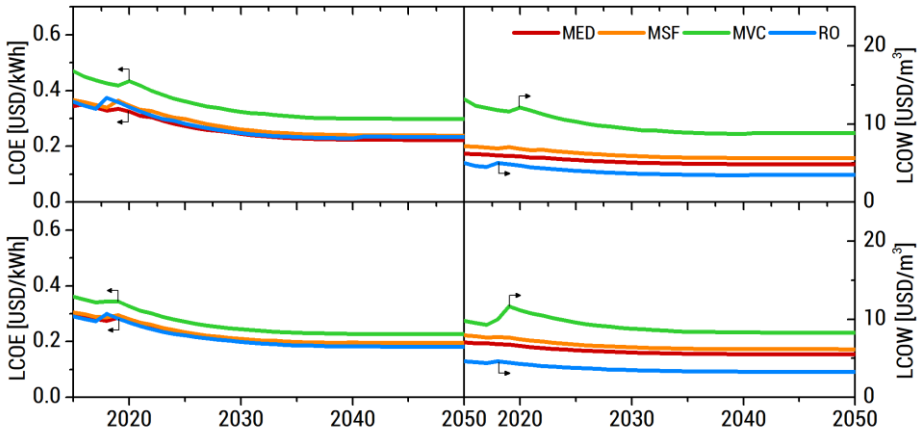

Figure 14. Projected LCOE and LCOW on Camasusu Island (**top**) and Lubang Island (**bottom**). The bumps near 2020 indicates a shift to a more RE-favored optimum configuration.

3.4. Sensitivity Analysis

3.4.1. −25% Overnight Fuel Cost

At a 25% decrease of the overnight diesel and coal price, the Li-ion BESS installation sizes sharply decreased, as shown by Figure 15. The bimodal distribution that was once present in MED and MVC systems in Camasusu have become a tight distribution, suggesting that RE-favored generation is no longer feasible. Systems on Lubang Island also favored diesel. Figure 16 also shows that all systems exhibit uncertainty in optimum storage sizes. Generation costs have decreased (Figure 17), especially for MVC, which consumes large quantities of diesel due to its high electrical energy intensity. Bimodal spreads of LCOE and LCOW have disappeared due to systems heavily favoring diesel over RE.

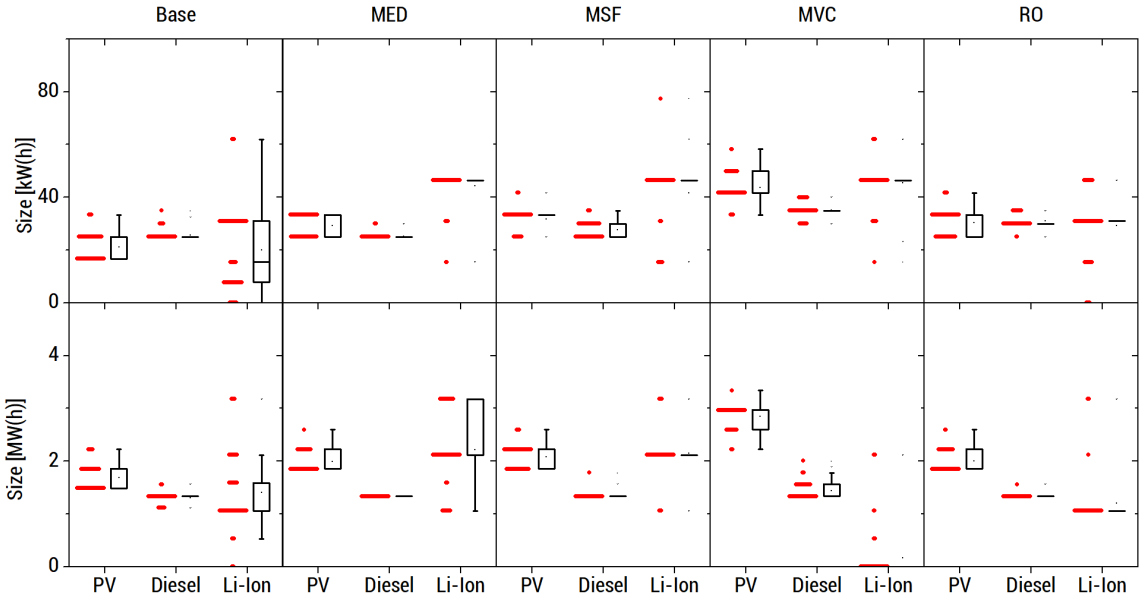

Figure 15. Distribution of optimum sizes of energy components on Camasusu Island (**top**) and Lubang Island (**bottom**) at −25% overnight fuel price.

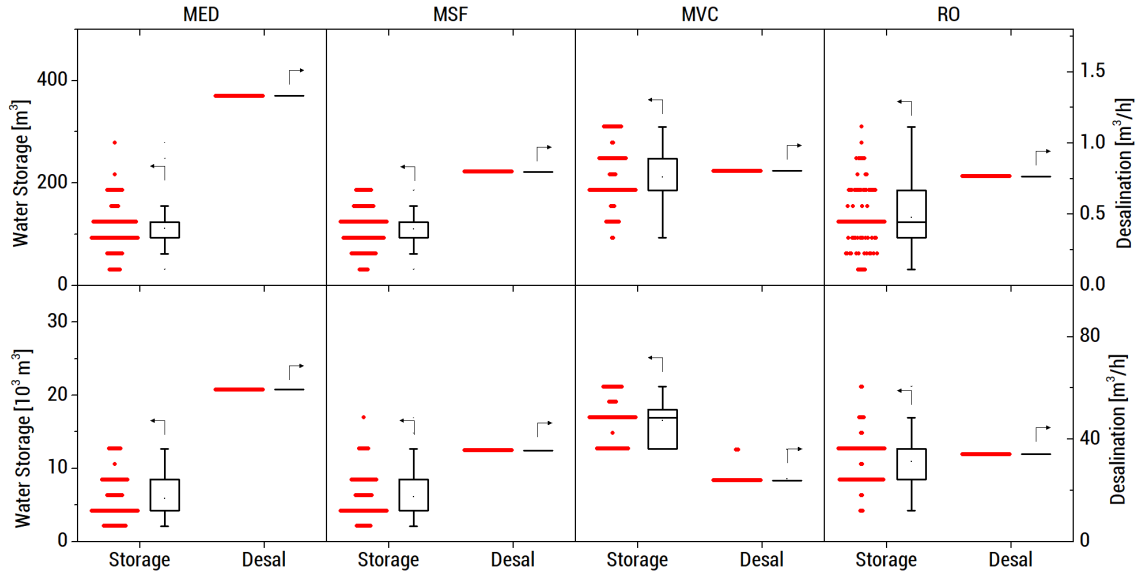

Figure 16. Distribution of optimum sizes of water storage and desalination unit on Camasusu Island (**top**) and Lubang Island (**bottom**) at −25% overnight fuel price. There is high uncertainty in the optimum water storage sizes in all systems on both islands.

3.4.2. +25% Overnight Fuel Cost

At a 25% increase in overnight diesel and coal cost, all systems have large Li-ion BESS installation sizes (Figure 18) preferring RE-favored generation due to prohibitive diesel costs. Figure 19 also shows minimal uncertainty in optimum storage sizes, confirming that RE-favored generation is favored. Generation costs have increased (Figure 20) especially in MVC systems, wherein diesel is used for energy generation, which in turn powers the MVC plant. This is less efficient that MED and MSF, which use the fuel directly.

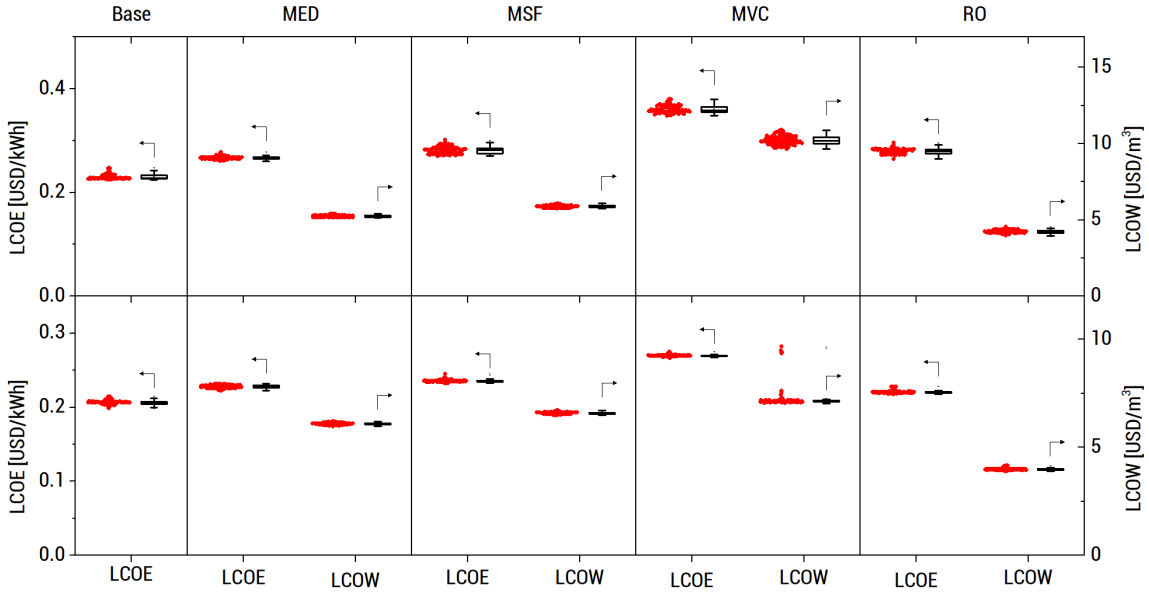

Figure 17. Distribution of optimum LCOE and LCOW on Camasusu Island (**top**) and Lubang Island (**bottom**) at −25% overnight fuel price. There is minimal uncertainty for these metrics.

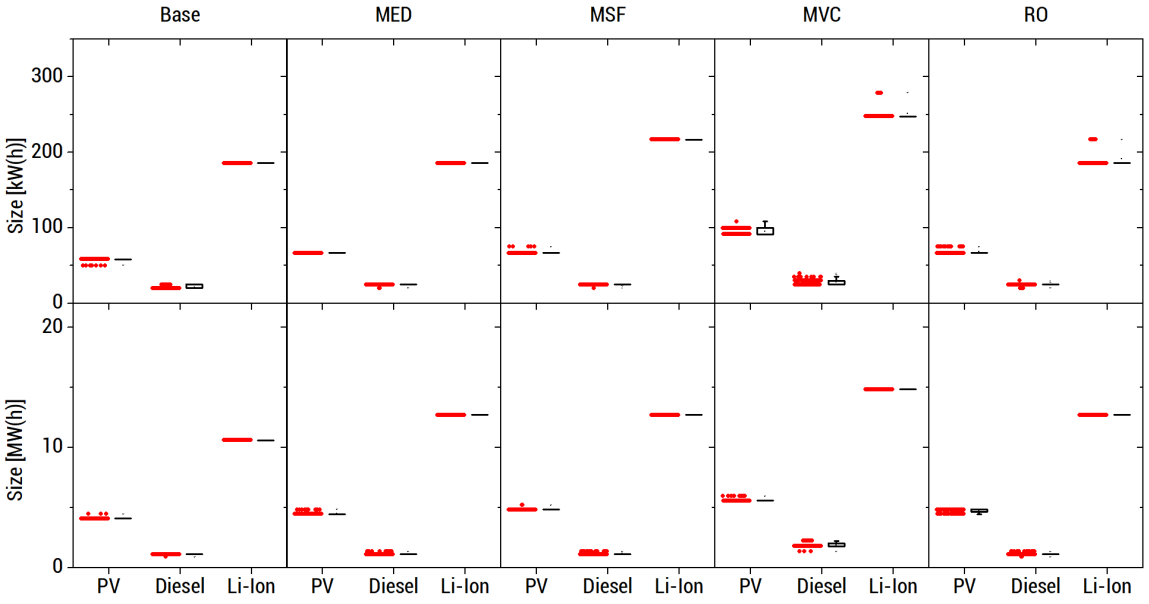

Figure 18. Distribution of optimum sizes of energy components on Camasusu Island (**top**) and Lubang Island (**bottom**) at +25% overnight fuel price.

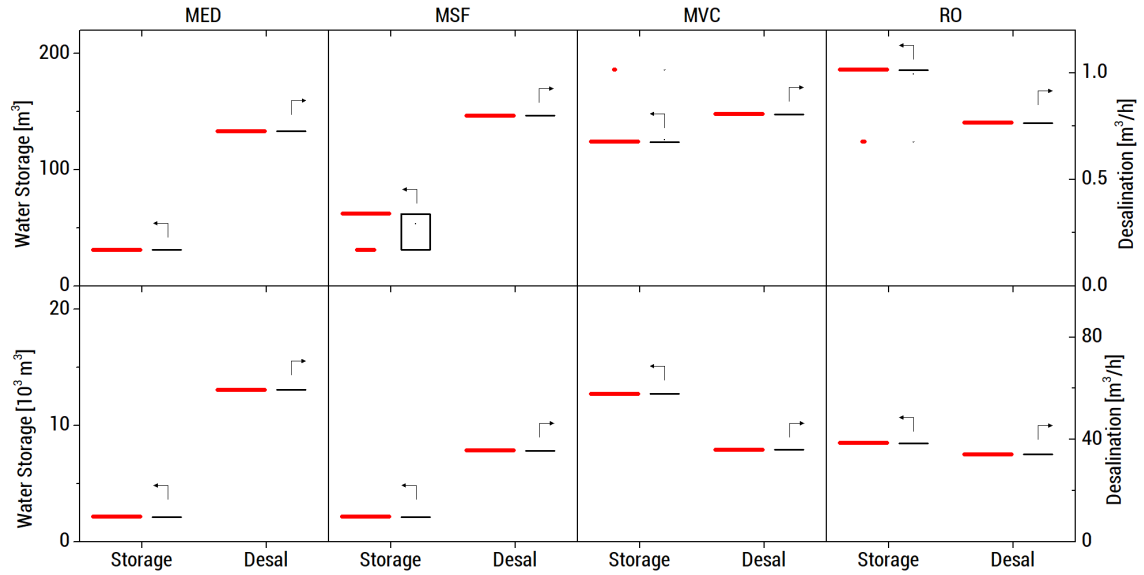

Figure 19. Distribution of optimum sizes of water storage and desalination unit on Camasusu Island (**top**) and Lubang Island (**bottom**) at +25% overnight fuel price. There is minimal uncertainty in optimum sizes in all systems on both islands.

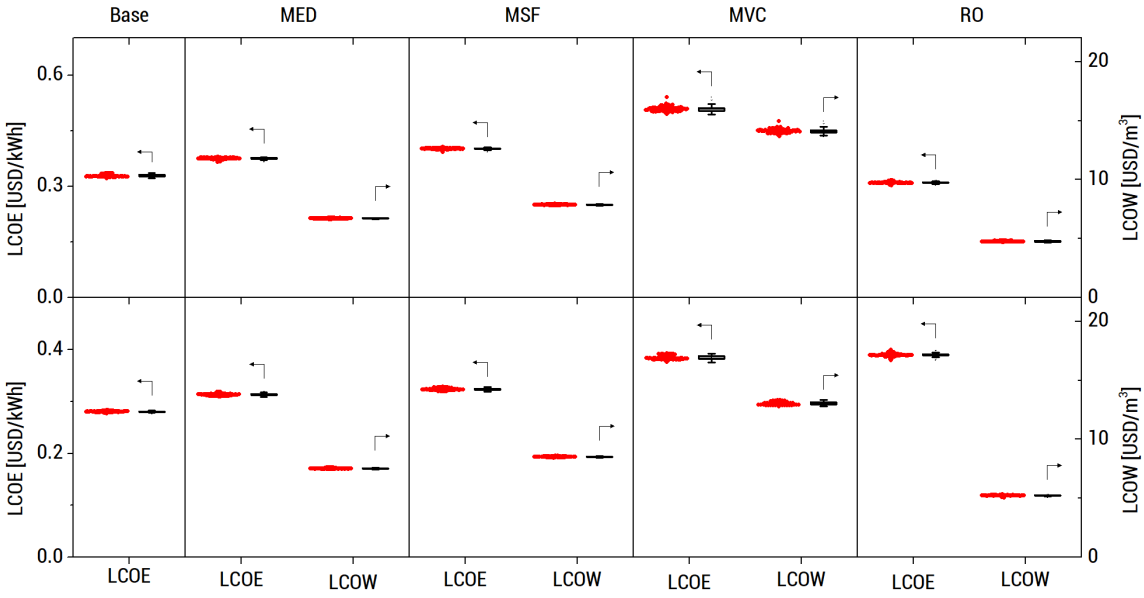

Figure 20. Distribution of optimum LCOE and LCOW for Camasusu Island (**top**) and Lubang Island (**bottom**) at +25% overnight fuel price. There is minimal uncertainty for these metrics.

4. Discussion

Upon analysis of the optimum size and metric distributions, RO systems have the lowest water generation cost. The low energy use and high turndown of RO allows for possible coupling with RE-favored generation. The average LCOW of RO systems is 5.11 USD/m^3 and 4.70 USD/m^3 for Camasusu and Lubang, respectively. Compared to the mainland price of 0.70 USD/m^3, however, water generation costs are still higher by 630% and 572% for Camasusu and Lubang, respectively. As for electricity generation costs, MED systems have the lowest average LCOE of 0.348 USD/kWh in Camasusu, while RO systems have the lowest average LCOE of 0.296 USD/kWh in Lubang. These are 74% and 47% more expensive for Camasusu and Lubang, respectively, compared to the mainland price of 0.2 USD/kWh [62]. Overall, RO systems provide cost-effective water and electricity, especially for larger islands, where RE-favored generation is preferred.

For project developers, MED and MSF could be more attractive because these systems are less RE-dependent than RO due to the limited turndown. This allows easier entry into off-grid islands currently powered by diesel generators. There is also less uncertainty in optimum sizes, especially for MSF, implying that there is less risk of installing an undersized system. Seasonal weather patterns also do not strongly affect the stored water level. Lastly, these technologies have smaller water storage sizes that are more appropriate for off-grid islands. However, due to the large typical sizes of MED and MSF plants, these technologies are favorable for larger islands only [44].

Energy-desalination systems on small islands prefer diesel-favored generation, while larger islands prefer RE-favored generation, as shown by the power flows. Cost projection analysis, however, suggests that RE-favored generation will be more favorable in the future even for small islands. RO desalination is therefore a favorable investment as its high turndown allows it to accept RE intermittency, in addition to its low generation costs. Given that most of the off-grid islands are currently powered by diesel generators [1] and that PV-based installations are gradually being deployed [63], energy-RO systems for energy and water cogeneration may be feasible in the near future.

The sensitivity analysis shows that energy-desalination system configurations heavily depend on diesel and coal prices. If fuel prices are low, the fuel share in thermal desalination systems increases and uncertainty in water storage installation size increases. Energy and water generation costs are reduced especially for MED, MSF, and MVC, as they rely on fuel. If fuel prices are high, RE-favored generation becomes favorable. There is less uncertainty in the optimum sizes of both energy and water components because Li-ion BESS energy storage minimizes intermittencies. However, large Li-ion BESS installations for RE-dominated generation result in high costs of energy and water.

In addition to the fuel dependence of the optimum configuration, the sensitivity analysis also has implications on system resiliency on fuel price shocks. If fuel prices were to surge upwards, the generation costs of RO systems will be affected the least due to its low dependence on fuel. MVC systems will have the largest increase in generation costs due to its inefficient fuel usage. Small islands are more susceptible to fuel price surges, as these tend to have diesel-favored energy systems. In contrast, large islands are more likely to have RE-favored generation, which is optimal at higher fuel prices. This incentivizes the implementation of RE-RO systems, as they are favorable for small islands and are resistant to fuel price shocks.

5. Conclusions

The RO desalination systems have favorable properties due to high turndown capabilities and low energy use. Coupled energy-RO systems provide a low energy generation cost and the lowest water generation cost due to the efficient energy use of RO. Its high turndown allows for compatibility with RE-favored generation and makes it a future-proof investment as RE installations increase in the future. RO-RE systems have greater resistance to fuel price surges, providing resiliency against the decreasing fuel supply and current political climate.

MED and MSF are easier to implement given the present configuration on off-grid islands in the Philippines. These desalination technologies are more compatible with diesel-favored generation, which is the status-quo on Philippine off-grid islands. The MED and MSF systems are robust against weather patterns, making them a viable investment in the Philippines. These technologies may also have niche applications where diesel prices are low or if small water storage units are preferable.

Author Contributions: Conceptualization, methodology, validation, and formal analysis was done by M.C. and J.O. Writing—original draft preparation was done by M.C. and M.A. Writing—review and editing and supervision was done by M.A., E.E.J., and J.O. Funding acquisition was done by J.O. All authors have read and agreed to the published version of the manuscript.

Funding: This research is part of the Energy Research Fund (ERF) project entitled "ElectriPHI—Electrification Planning in Small Off-grid Islands in the Philippines" funded through the University of the Philippines Office of the Vice-President for Academic Affairs (UP OVPAA) and the Senate Committee on Energy led by Sen. Sherwin T. Gatchalian.

Acknowledgments: J.O. would like to acknowledge the Federico Puno Professorial Chair Award and the US-ASEAN Science & Technology Fellowship. M.C. would like to acknowledge the Department of Science and Technology Science Education Institute (DOST-SEI) Merit Scholarship Program.

Conflicts of Interest: The authors declare no conflict of interest.

Appendix A

A.1. Energy System Models

A.1.1. Solar PV

The power output of the solar system is given by Equation (A1). It is proportional to the incident radiation on the tilted surface $G(t)$ and is partly influenced by the cell temperature $T_C(t)$. Details regarding the calculation of these parameters can be found in [64]. In Equation (A1), S_{PV} is the rated size of the solar PV installation, η_{PV} is the derating factor (0.8), G_{STC} is the irradiance at standard test conditions (STC, 1 kW/m^2), α_P is the temperature coefficient of power (−0.005 K^{-1}), and T_{STC} is the temperature at STC.

$$P_{PV}(t) = S_{PV}\eta_{PV}\frac{G(t)}{G_{STC}}[1 + \alpha_P(T_C(t) - T_{STC})], \tag{A1}$$

A.1.2. Diesel

Diesel generators can output any power below its rated size S_{ds}. A minimum power ratio r (0.1) is implemented and the minimum power output of a diesel generator is given by Equation (A2):

$$P_{ds}^{min}(t) = rS_{ds}, \tag{A2}$$

The amount of fuel consumed by the plant is directly proportional to the rated size and the power output $P_{ds}(t)$ as given by Equation (A3). Both C_0 and C_1 are arbitrary constants [65].

$$\dot{V}_{fl}(t) = C_0 S_{ds} + C_1 P_{ds}(t), \tag{A3}$$

The fuel efficiency is given by Equation (A4), wherein ρ is the density of diesel (820 kg/m^3) and ΔH_{LHV} is the lower heating value of diesel (43.2 MJ/kg). The efficiency is specified as 0.3 and 0.4 at the minimum and maximum loading, respectively. This allows the coefficients in Equation (A3) to be determined.

$$\eta_{ds}(t) = \frac{P_{ds}(t)}{\rho \dot{V}_{ds}(t)\Delta H_{LHV}}, \tag{A4}$$

A.1.3. Li-Ion BESS

The charging and discharging rate of the Li-ion BESS is limited by either the C-rate or the state of charge (SOC) as shown by Equations (A5) and (A6). In these equations, S_{Li} is the rated size of the Li-ion BESS installation, C is the C-rate, and the $\min\{x, y\}$ function returns whichever is smaller among x or y. The negative sign indicates charging, as this will be relevant in the later equations. In Equation (A6), a maximum depth of discharge ($\text{DOD}_{\max}$) of 0.8 is implemented as too much discharge that will damage the BESS:

$$P_c^{max}(t) = -\min\left\{ \; S_{Li}C, \quad S_{Li}(1 - \text{SOC}(t)) \; \right\}, \tag{A5}$$

$$P_{dc}^{max}(t) = \min\left\{ \; S_{Li}C, \quad S_{Li}(\text{SOC} - (1 - \text{DOD}_{\max})) \; \right\}, \tag{A6}$$

Next, the power entering one battery module $P(t)$ is determined as shown in Equations (A7) and (A8) for charging and discharging, respectively. A charge ϵ_c and discharge ϵ_{dc} efficiency of 0.95 is

applied, which results in a roundtrip efficiency of 0.90 when combined. S_{nom} is the nominal size of one battery module (4.8 kWh).

$$P(t) = \frac{P_c(t)\epsilon_c}{S_{st}/S_{nom}}, \tag{A7}$$

$$P(t) = \frac{P_{dc}(t)/\epsilon_{dc}}{S_{st}/S_{nom}}, \tag{A8}$$

The Li-ion battery chemistry is modeled using the Thevenin equivalent circuit as shown in Figure A1. $P(t)$ represents the power at the terminals. R_1 (1.4 Ω) is the resistance due to the electrolyte, while R_2 (0.5 Ω) and C (52 F) are resistances at the electrode interface [66].

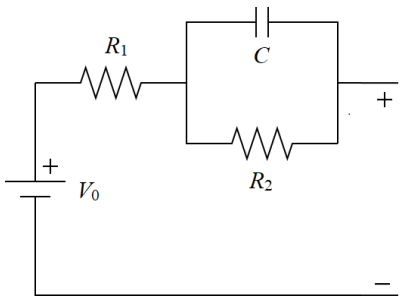

Figure A1. Thevenin equivalent circuit for modelling Li-ion battery chemistry.

The current through the EMF element is determined and the SOC for the next timestep is given by Equation (A9). $V_0(t)$ is the open circuit voltage (OCV) of the battery module.

$$\mathrm{SOC}(t+1) = \mathrm{SOC}(t) - \frac{I(t)V_0(t)}{S_{nom}}, \tag{A9}$$

The module OCV is given as a function of SOC by Figure A2.

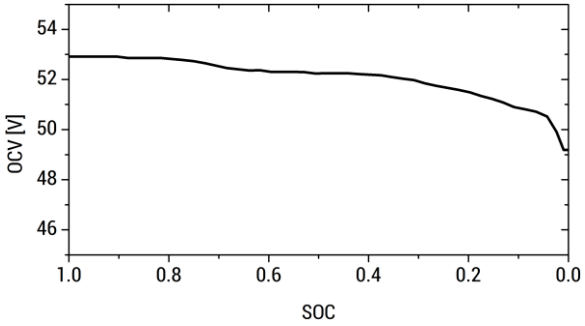

Figure A2. Open circuit voltage (OCV) as a function of SOC for a 48 V Li-ion battery module.

A.2. Dispatch Algorithm

The dispatch algorithm decides how energy is distributed throughout the system. ISLA uses a load-following dispatch algorithm that has been modified to accommodate desalination as shown in Figure A3. First, the algorithm checks if solar PV power at that timestep can supply both the electrical demand and desalination power. If so, the BESS is charged, and any more excess power is absorbed by the desalination plant. Otherwise, power is drawn from the Li-ion BESS. If the Li-ion BESS does not suffice, additional diesel generation is called. If this still does not suffice, then a power outage is declared, and the system is infeasible.

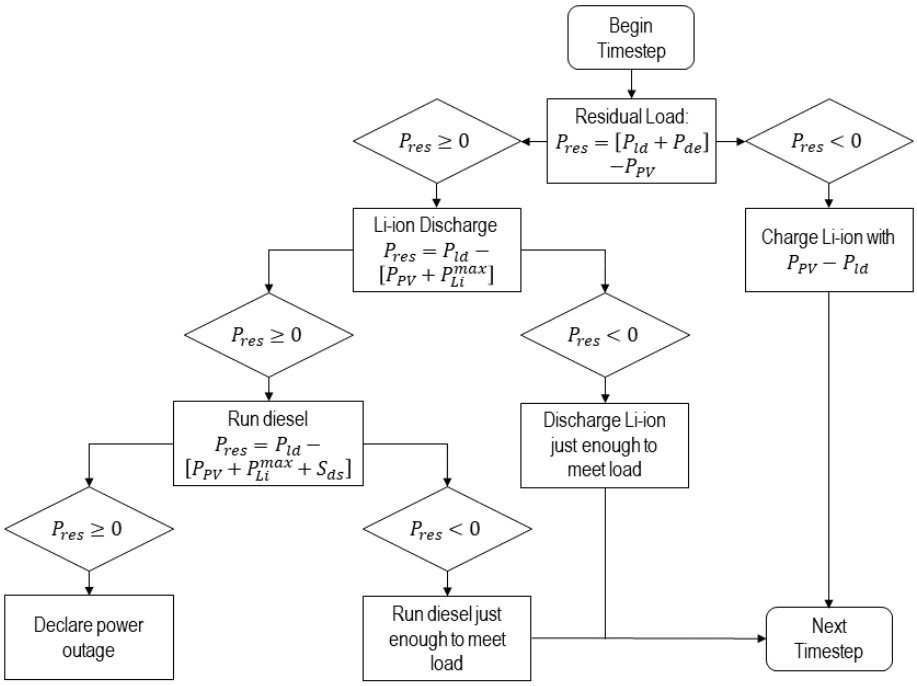

Figure A3. Load-following dispatch algorithm used by ISLA. To reduce carbon emissions, the system prioritizes the usage of stored Li-ion BESS energy over diesel power if solar PV power is insufficient.

Appendix B

To ensure that a physically sensible optimum is obtained, the initial search space must be generated properly. The procedure below shows how ISLA generates the initial search space, but this does not guarantee a global optimum value as with nonlinear optimization problems. Nonetheless, the results generated by ISLA for energy-only microgrid systems were consistent with those from HOMER Pro®.

The sizes of solar PV, diesel, and the desalination unit are rated based on their maximum power [kW] or flowrate [m^3/h] generation, thus, the optimum value must be based on the peak demand. A crude approximation of the peak electrical demand P_{pk} is calculated as shown in Equation (A10). The constant 10 kW/(m^3/h) was arbitrarily chosen such that it is near the electrical energy intensities EI_{el} of the desalination units in this study.

$$P_{pk} = \max\left\{P_{ld}(t) + \frac{10\ \text{kW}}{\text{m}^3/\text{h}}\dot{V}_{ld}(t)\right\}, \tag{A10}$$

The initial search spaces of solar PV $\{S_{PV}\}_0$, diesel $\{S_{ds}\}_0$, and the desalination unit $\{S_{de}\}_0$ are shown in Equations (A11)–(A13). Constants are multiplied to P_{pk} due to the possibility of the optimum size deviating from the crudely approximated peak demand. The diesel generator has a small associated constant because its optimum size must be near the peak demand. Smaller sizes may be technically infeasible, while larger sizes will incur high capital cost. Solar PV has a larger associated constant because it has power peaks during the day that are much larger than the peak demand.

$$\{S_{PV}\}_0 = \left[\ 0,\quad 5P_{pk}\ \right], \tag{A11}$$

$$\{S_{ds}\}_0 = \left[\ 0,\quad 3P_{pk}\ \right], \tag{A12}$$

$$\{S_{de}\}_0 = \left[\ 0,\quad \frac{2P_{pk}}{\text{EI}_{\text{el}}}\ \right], \tag{A13}$$

The Li-ion BESS and water storage undergo daily cycles of influx and efflux; thus, it is unlikely to have a Li-ion BESS or water storage that drains in less than a day. Their search spaces are therefore

based on daily consumption. A crude approximation of the daily power consumption E_{dy} is given by Equation (A14). Compared to Equation (A10), a smaller constant of 5 kW/(m^3/h) was chosen because the average daily power consumption is less sensitive to sharp peaks in the actual demand profile.

$$E_{dy} = \frac{1}{365}\left[\sum_{i=0}^{8759} P_{ld}(t)\Delta t + \frac{5\,\text{kW}}{\text{m}^3/\text{h}} \cdot \sum_{i=0}^{8759} \dot{V}_{ld}(t)\Delta t\right], \tag{A14}$$

The initial search spaces of Li-ion BESS $\{S_{Li}\}_0$ and water storage $\{S_{tank}\}_0$ are shown in Equations (A15) and (A16). Constants are multiplied to E_{dy} due to the possibility of the optimum size deviating from the crudely approximated daily energy consumption. These constants are smaller, however, because caution against sharp peaks in the actual demand profile is unnecessary.

$$\{S_{Li}\}_0 = \left[\ 0, \quad 2E_{dy}\ \right], \tag{A15}$$

$$\{S_{tank}\}_0 = \left[\ 0, \quad \frac{2E_{dy}}{\text{EI}_{\text{el}}}\ \right], \tag{A16}$$

Appendix C

The techno-economic parameters of the energy generation components are shown in Table A1. These parameters are valid for the year 2015.

Table A1. Techno-economic parameters of energy components.

Component	Parameter	Unit	Value	Ref.
PV	CapEx	USD/kW	1200	[67]
	OpEx	USD/kW/y	25	
	Lifetime	y	20	[68]
Li-ion BESS	CapEx	USD/kWh	300	[69]
	OpEx	USD/kWh/y	3	
	Lifetime	y	10	
	RT Efficiency	%	90	
Diesel Generator	CapEx	USD/kW	500	
	OpEx	USD/kWh	0.03	
	Lifetime	h	15,000	
Diesel	Cost	USD/L	0.9	
	Inflation Rate	%	3	
Project	CapEx	USD	0	
	OpEx	USD/y	0	
	Discount Rate	%	10	
	Lifetime	y	20	

Appendix D

The future cost parameters of energy components are summarized in Table A2.

Table A2. Future cost parameters of energy components.

Component	K [GW(h)]	r [y^{-1}]	t_m [y]	Ref.	b	Ref.
PV	200	1.7362	2004	[6]	0.376	[6]
Li-ion BESS	2600	2.7363	2011	[6]	0.251	[6]

Appendix E

The global horizontal irradiance (GHI), energy demand, and water demand of Camasusu Island and Lubang Island are shown in Figures A4 and A5, respectively. The GHI profiles were obtained from PHIL-LIDAR 2 dataset, while the electrical demand load profiles were obtained from the work of Navarro [70].

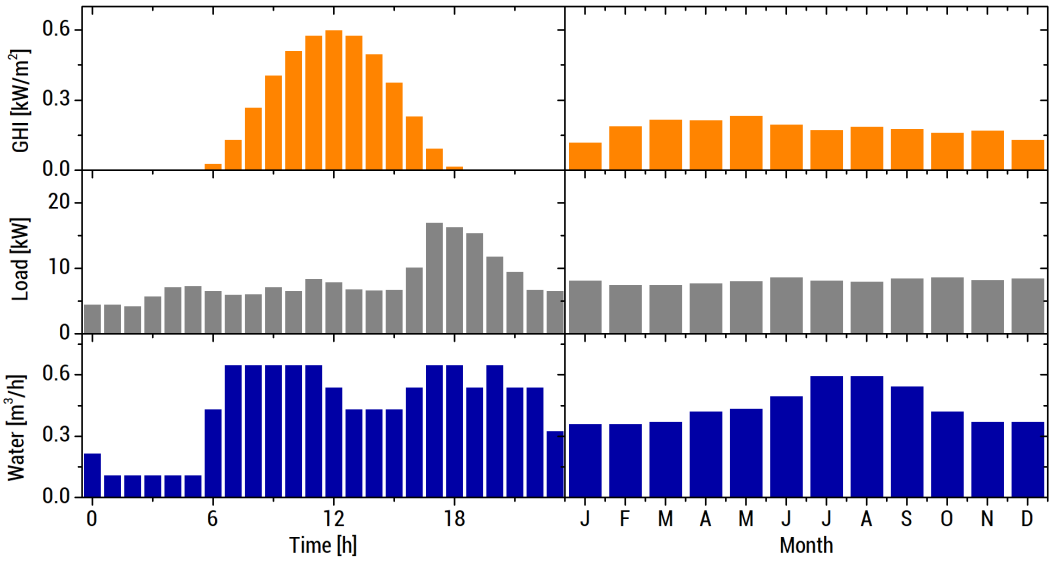

Figure A4. Daily and monthly average electric, water, and GHI profiles on Camasusu Island.

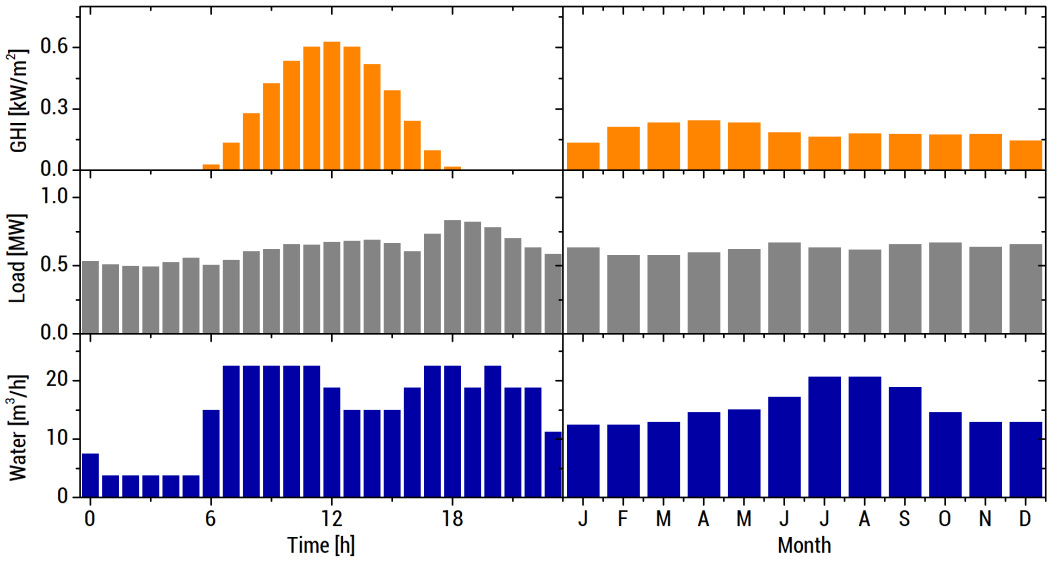

Figure A5. Daily and monthly average electric, water, and GHI profiles on Lubang Island.

References

1. Ocon, J.D.; Bertheau, P. Energy Transition from Diesel-based to Solar Photovoltaics-Battery-Diesel Hybrid System-based Island Grids in the Philippines—Techno-Economic Potential and Policy Implication on Missionary Electrification. *J. Sustain. Dev. Energy Water Environ. Syst.* **2019**, *7*, 139–154. [CrossRef]
2. Holding, S.; Allen, D.M.; Foster, S.; Hsieh, A.; Larocque, I.; Klassen, J.; Van Pelt, S.C. Groundwater vulnerability on small islands. *Nat. Clim. Chang.* **2016**, *6*, 1100–1103. [CrossRef]
3. NEA to Give Romblons Cobrador Island Potable Water Thru Hydropanels. Available online: https://www.ikot.ph/nea-to-give-romblons-cobrador-island-potable-water-thru-hydropanels (accessed on 24 April 2020).

4. International Labor Organization. *Report V: Sustainable Development, Decent Work and Green Jobs*; International Labor Organization: Geneva, Switzerland, 2013.
5. Lilane, A.; Saifaoui, D.; Hariss, S.; Jenkal, H.; Chouiekh, M. Modeling and simulation of the performances of the reverse osmosis membrane. *Mater. Today Proc.* **2019**, *24*, 114–118. [CrossRef]
6. Schmidt, O.; Hawkes, A.; Gambhir, A.; Staffell, I. The future cost of electrical energy storage based on experience rates. *Nat. Energy* **2017**, *2*, 1–8. [CrossRef]
7. Schmidt, O.; Melchior, S.; Hawkes, A.; Staffell, I. Projecting the Future Levelized Cost of Electricity Storage Technologies. *Joule* **2019**, *3*, 81–100. [CrossRef]
8. Bajpai, P.; Dash, V. Hybrid renewable energy systems for power generation in stand-alone applications: A review. *Renew. Sustain. Energy Rev.* **2012**, *16*, 2926–2939. [CrossRef]
9. Bertheau, P.; Blechinger, P. Resilient solar energy island supply to support SDG7 on the Philippines: Techno-economic optimized electrification strategy for small islands. *Util. Policy* **2018**, *54*, 55–77. [CrossRef]
10. Fernández-Gil, G.; Petrakopoulou, F. Sustainable water generation on a mediterranean island in Greece. *Energies* **2019**, *12*, 4247. [CrossRef]
11. Tafech, A.; Milani, D.; Abbas, A. Water storage instead of energy storage for desalination powered by renewable energy—King Island case study. *Energies* **2016**, *9*, 839. [CrossRef]
12. Philstar Global Water Rates up in July 2018. Available online: https://www.philstar.com/headlines/2018/06/15/1824833/water-rates-july-2018 (accessed on 24 April 2020).
13. Gökçek, M. Integration of hybrid power (wind-photovoltaic-diesel-battery) and seawater reverse osmosis systems for small-scale desalination applications. *Desalination* **2018**, *435*, 210–220. [CrossRef]
14. Corsini, A.; Tortora, E. Sea-Water Desalination for Load Levelling of Gen-Sets in Small Off-Grid Islands. *Energies* **2018**, *11*, 2068. [CrossRef]
15. Bognar, K.; Pohl, R.; Behrendt, F. Seawater reverse osmosis (SWRO) as deferrable load in micro grids. *Desalin. Water Treat.* **2013**, *51*, 1190–1199. [CrossRef]
16. International Atomic Energy Agency. *Use of Nuclear Reactors for Seawater Desalination*; International Atomic Energy Agency: Vienna, Austria, 1990.
17. Khalifa, A.J.N. Evaluation of different hybrid power scenarios to Reverse Osmosis (RO) desalination units in isolated areas in Iraq. *Energy Sustain. Dev.* **2011**, *15*, 49–54. [CrossRef]
18. Azinheira, G.; Segurado, R.; Costa, M. Is renewable energy-powered desalination a viable solution for water stressed regions? A case study in Algarve, Portugal. *Energies* **2019**, *12*, 4651. [CrossRef]
19. Rao, P.; Morrow, W.R.; Aghajanzadeh, A.; Sheaffer, P.; Dollinger, C.; Brueske, S.; Cresko, J. Energy considerations associated with increased adoption of seawater desalination in the United States. *Desalination* **2018**, *445*, 213–224. [CrossRef]
20. Qiu, T.; Davies, P.A. Comparison of configurations for high-recovery inland desalination systems. *Water* **2012**, *4*, 690–706. [CrossRef]
21. Monterrey-Viña, A.; Musicki-Savic, A.; Díaz-Peña, F.J.; Peñate-Suárez, B. Technical and agronomical assessment of the use of desalinated seawater for coastal irrigation in an insular context. *Water* **2020**, *12*, 272. [CrossRef]
22. Caldera, U.; Breyer, C. Learning Curve for Seawater Reverse Osmosis Desalination Plants: Capital Cost Trend of the Past, Present, and Future. *Water Resour. Res.* **2017**, *53*, 10523–10538. [CrossRef]
23. Jones, E.; Qadir, M.; van Vliet, M.T.H.; Smakhtin, V.; Kang, S. mu The state of desalination and brine production: A global outlook. *Sci. Total Environ.* **2019**, *657*, 1343–1356. [CrossRef]
24. Ullah, I.; Rasul, M.G. Recent developments in solar thermal desalination technologies: A review. *Energies* **2019**, *12*, 119. [CrossRef]
25. Reddy, K.V.; Ghaffour, N. Overview of the cost of desalinated water and costing methodologies. *Desalination* **2007**, *205*, 340–353. [CrossRef]
26. Mayor, B. Growth patterns in mature desalination technologies and analogies with the energy field. *Desalination* **2019**, *457*, 75–84. [CrossRef]
27. Sood, A.; Smakhtin, V. Can desalination and clean energy combined help to alleviate global water scarcity? *J. Am. Water Resour. Assoc.* **2014**, *50*, 1111–1123. [CrossRef]
28. Ahmadvand, S.; Abbasi, B.; Azarfar, B.; Elhashimi, M.; Zhang, X.; Abbasi, B. Looking beyond energy efficiency: An applied review of water desalination technologies and an introduction to capillary-driven desalination. *Water* **2019**, *11*, 696. [CrossRef]

29. Williams, E.; Hittinger, E.; Carvalho, R.; Williams, R. Wind power costs expected to decrease due to technological progress. *Energy Policy* **2017**, *106*, 427–435. [CrossRef]
30. Maqbool, N.; Saleem, Z.; Jamal, Y. Open Access Journal of Waste Management & Xenobiotics A Short Review on A Short Review on Reverse Osmosis Membranes: Fouling and Control. *A Short Rev. Reverse Osmosis Membr. Fouling Control* **2019**, *2*. [CrossRef]
31. Coutinho de Paula, E.; Amaral, M.C.S. Extending the life-cycle of reverse osmosis membranes: A review. *Waste Manag. Res.* **2017**, *35*, 456–470. [CrossRef]
32. Yang, Z.; Zhou, Y.; Feng, Z.; Rui, X.; Zhang, T.; Zhang, Z. A review on reverse osmosis and nanofiltration membranes for water purification. *Polymers* **2019**, *11*, 1252. [CrossRef]
33. Ruiz-García, A.; Melián-Martel, N.; Nuez, I. Short review on predicting fouling in RO desalination. *Membranes* **2017**, *7*, 62. [CrossRef]
34. Al-Amshawee, S.; Yunus, M.Y.B.M.; Azoddein, A.A.M.; Hassell, D.G.; Dakhil, I.H.; Hasan, H.A. Electrodialysis desalination for water and wastewater: A review. *Chem. Eng. J.* **2020**, *380*, 122231. [CrossRef]
35. Carballo, J.A.; Bonilla, J.; Roca, L.; De la Calle, A.; Palenzuela, P.; Alarcón-Padilla, D.C. Optimal operating conditions analysis for a multi-effect distillation plant according to energetic and exergetic criteria. *Desalination* **2018**, *435*, 70–76. [CrossRef]
36. Nannarone, A.; Toro, C.; Sciubba, E. Multi-stage flash desalination process: Modeling and simulation. In Proceedings of the 30th International Conference on Efficiency, Cost, Optimization, Simulation and Environmental Impact of Energy Systems-ECOS 2017, San Diego, CA, USA, 2–6 July 2017.
37. El-Feky, A.K. Mechanical Vapor Compression (MVC) Desalination System Optimal Design. *Arab J. Nucl. Sci. Appl.* **2016**, *94*, 1–13.
38. Jamil, M.A.; Zubair, S.M. On thermoeconomic analysis of a single-effect mechanical vapor compression desalination system. *Desalination* **2017**, *420*, 292–307. [CrossRef]
39. Namany, S.; Al-Ansari, T.; Govindan, R. Optimisation of the energy, water, and food nexus for food security scenarios. *Comput. Chem. Eng.* **2019**, *129*, 106513. [CrossRef]
40. Mandelli, S.; Brivio, C.; Colombo, E.; Merlo, M. Effect of load profile uncertainty on the optimum sizing of off-grid PV systems for rural electrification. *Sustain. Energy Technol. Assess.* **2016**, *18*, 34–47. [CrossRef]
41. Castro, M.T.; Esparcia, E.A.; Odulio, C.M.F.; Ocon, J.D. Technoeconomics of reverse osmosis as demand-side management for Philippine off-grid islands. *Chem. Eng. Trans.* **2019**, *76*, 1129–1134.
42. Gökçek, M.; Gökçek, Ö.B. Technical and economic evaluation of freshwater production from a wind-powered small-scale seawater reverse osmosis system (WP-SWRO). *Desalination* **2016**, *381*, 47–57. [CrossRef]
43. Ozonoh, M.; Aniokete, T.C.; Oboirien, B.O.; Daramola, M.O. Techno-economic analysis of electricity and heat production by co-gasification of coal, biomass and waste tyre in South Africa. *J. Clean. Prod.* **2018**, *201*, 192–206. [CrossRef]
44. Abdelkareem, M.A.; El Haj Assad, M.; Sayed, E.T.; Soudan, B. Recent progress in the use of renewable energy sources to power water desalination plants. *Desalination* **2018**, *435*, 97–113. [CrossRef]
45. Ghalavand, Y.; Hatamipour, M.S.; Rahimi, A. A review on energy consumption of desalination processes. *Desalin. Water Treat.* **2015**, *54*, 1526–1541. [CrossRef]
46. Ghaffour, N.; Missimer, T.M.; Amy, G.L. Technical review and evaluation of the economics of water desalination: Current and future challenges for better water supply sustainability. *Desalination* **2013**, *309*, 197–207. [CrossRef]
47. Aquatech International Corporation. *Case Study: Seawater Desalination at Rabigh Refinery*; Aquatech International Corporation: Canonsburg, PA, USA, 2020.
48. Rahimi, B.; Chua, H. *Low Grade Heat Driven Multi-effect Distillation and Desalination*, 1st ed.; Elsevier: Amsterdam, The Netherlands, 2017.
49. Elsayed, M.L.; Mesalhy, O.; Mohammed, R.H.; Chow, L.C. Transient and thermo-economic analysis of MED-MVC desalination system. *Energy* **2019**, *167*, 283–296. [CrossRef]
50. Kim, J.S.; Garcia, H.E. *Hybrid Energy: Combining Nuclear and Other Energy Sources*; Idaho National Lab. (INL): Idaho Falls, ID, USA, 2015.
51. Papapetrou, M.; Cipollina, A.; La Commare, U.; Micale, G.; Zaragoza, G.; Kosmadakis, G. Assessment of methodologies and data used to calculate desalination costs. *Desalination* **2017**, *419*, 8–19. [CrossRef]
52. Lara, J.; Osunsan, O.; Holtzapple, M. Advanced mechanical vapor-compression desalination system. In *Desalination, Trends and Technologies*; Schorr, M., Ed.; IntechOpen: London, UK, 2012.

53. De Andrade Cruz, M.; Araújo, O.d.Q.F.; de Medeiros, J.L.; de Castro, R.d.P.V.; Ribeiro, G.T.; de Oliveira, V.R. Impact of solid waste treatment from spray dryer absorber on the levelized cost of energy of a coal-fired power plant. *J. Clean. Prod.* **2017**, *164*, 1623–1634. [CrossRef]
54. Wang, F.; Deng, S.; Zhao, J.; Zhao, J.; Yang, G.; Yan, J. Integrating geothermal into coal-fired power plant with carbon capture: A comparative study with solar energy. *Energy Convers. Manag.* **2017**, *148*, 569–582. [CrossRef]
55. Mayor, B. Unraveling the Historical Economies of Scale and Learning Effects for Desalination Technologies. *Water Resour. Res.* **2020**, *56*, 1–10. [CrossRef]
56. Cipollina, A.; Micale, G.; Rizzuti, L. *Seawater Desalination: Conventional and Renewable Energy Processes*; Springer: Berlin, Germany, 2012; ISBN 9781608054220.
57. California Public Utilities Commission. *Embedded Energy in Water Studies Study 3: End Use Water Demand Profiles*; California Public Utilities Commission: San Francisco, CA, USA, 2011.
58. Griffin, R.C.; Chang, C. Seasonality in Community Water Demand. *West. J. Agric. Econ.* **1991**, *16*, 207–217.
59. Bendt, P.; Collares-Pereira, M.; Rabl, A. The frequency distribution of daily insolation values. *Sol. Energy* **1981**, *27*, 1–5. [CrossRef]
60. Graham, V.A.; Hollands, K.G.T.; Unny, T.E. A time series model for Kt with application to global synthetic weather generation. *Sol. Energy* **1988**, *40*, 83–92. [CrossRef]
61. Graham, V.A.; Hollands, K.G.T. A method to generate synthetic hourly solar radiation globally. *Sol. Energy* **1990**, *44*, 333–341. [CrossRef]
62. MERALCO Local DU Rate. Available online: www.meralco.com.ph (accessed on 24 April 2020).
63. National Power Corporation NPC Holds Groundbreaking of Solar Power Plant in Limasawa Island. Available online: https://www.napocor.gov.ph/index.php/news/archived-news/189-npc-holds-groundbreaking-of-solar-power-plant-in-limasawa-island (accessed on 24 April 2020).
64. Duffie, J.; Beckman, W. *Solar Engineering of Thermal Processes*; Wiley: New York, NY, USA, 2013; ISBN 9780470873663.
65. McGowan, J.G.; Manwell, J.F.; Connors, S.R. Wind/diesel energy systems: Review of design options and recent developments. *Sol. Energy* **1988**, *41*, 561–575. [CrossRef]
66. He, H.; Xiong, R.; Fan, J. Evaluation of lithium-ion battery equivalent circuit models for state of charge estimation by an experimental approach. *Energies* **2011**, *4*, 582–598. [CrossRef]
67. Fu, R.; Feldman, D.; Margolis, R. *US Solar Photovoltaic System Cost Benchmark: Q1 2018*; NREL/TP-6A20-72399; National Renewable Energy Laboratory: Golden, CO, USA, 2018.
68. Blechinger, P. *Barriers and Solutions to Implementing Renewable Energies on Caribbean Islands in Respect of Technical, Economic, Political, and Social Conditions, Schriftenreihe der Reiner Lemoine-Stiftung*; Shaker Verlag: Herzogenrath, Germany, 2015.
69. Diorio, N.; Dobos, A.; Janzou, S.; Nelson, A.; Lundstrom, B. *Technoeconomic Modeling of Battery Energy Storage in SAM*; NREL Technical Report; National Renewable Energy Laboratory: Golden, CO, USA, 2015.
70. Navarro, S. Hybrid opportunities in SPUG areas using HOMER. In Proceedings of the Asian Clean Energy Forum, Manila, Philippines, 6–10 June 2016.